NeuroImage 98 (2014) 233–242

Contents lists available at ScienceDirect

NeuroImage

journal homepage: www.elsevier.com/locate/ynimg

Impaired functional organization in the visual cortex of muscarinic receptor knock-out mice

Marianne Groleau [a,b], Hoang Nam Nguyen [a], Matthieu P. Vanni [b], Frédéric Huppé-Gourgues [a], Christian Casanova [b], Elvire Vaucher [a,*]

[a] Laboratoire de Neurobiologie de la Cognition Visuelle, École d'optométrie, Université de Montréal, Montréal, Québec, Canada
[b] Laboratoire des Neurosciences de la Vision, École d'optométrie, Université de Montréal, Montréal, Québec, Canada

ARTICLE INFO

Article history:
Accepted 7 May 2014
Available online 14 May 2014

Keywords:
Cartography
Muscarinic receptors
Visual cortex
Cortical activity

ABSTRACT

Acetylcholine modulates maturation and neuronal activity through muscarinic and nicotinic receptors in the primary visual cortex. However, the specific contribution of different muscarinic receptor subtypes in these neuromodulatory mechanisms is not fully understood. The present study evaluates in vivo the functional organization and the properties of the visual cortex of different groups of muscarinic receptor knock-out (KO) mice. Optical imaging of intrinsic signals coupled to continuous and episodic visual stimulation paradigms was used. Retinotopic maps along elevation and azimuth were preserved among the different groups of mice. However, compared to their wild-type counterparts, the apparent visual field along elevation was larger in M2/M4-KO mice but smaller in M1-KO. There was a reduction in the estimated relative receptive field size of V1 neurons in M1/M3-KO and M1-KO mice. Spatial frequency and contrast selectivity of V1 neuronal populations were affected only in M1/M3-KO and M1-KO mice. Finally, the neuronal connectivity was altered by the absence of M2/M4 muscarinic receptors. All these effects suggest the distinct roles of different subtypes of muscarinic receptors in the intrinsic organization of V1 and a strong involvement of the muscarinic transmission in the detectability of visual stimuli.

Introduction

The cerebral cholinergic system contributes to fine tuning of the sensory cortex during development, maturation and structure–function plasticity. In the primary visual cortex (V1), acetylcholine (ACh) modulates the neuron responses to new visual stimuli (Amar et al., 2010; Bear and Singer, 1986; Collier and Mitchell, 1966; Laplante et al., 2005; Thiele, 2013), the orientation selectivity of single cells and the orientation and direction selectivity of complex cells (Bhattacharyya et al., 2013; Murphy and Sillito, 1991; Sato et al., 1987; Zinke et al., 2006). Its neuromodulatory action mediates the attentional enhancement of specific visual stimuli processing (Herrero et al., 2008), and long-term modification of the neuronal responses (Dringenberg et al., 2007; Greuel et al., 1988; Heynen and Bear, 2001; Kang and Vaucher, 2009), leading to the functional plasticity and perceptual learning (Kang et al., 2013). The deficit of ACh in V1 leads to a decreased cortical responsiveness to visual stimuli as seen by c-Fos immunoreactivity (Dotigny et al., 2008).

These functions are mediated through two major classes of cholinergic receptors namely muscarinic (mAChR) and nicotinic (nAChR) receptors located at every level of the cortical microcircuitry (Disney et al., 2006; Prusky et al., 1987; Soma et al., 2012; Volpicelli and Levey, 2004). Although nAChRs are involved in the facilitation of glutamatergic transmission at V1 thalamo-cortical synapses (Gil et al., 1997), the present study focuses on mAChRs since they are involved in long-term mechanisms in V1. Five G-protein-coupled mAChR genes (*m1–m5*) have been characterized, each encoding a different subtype of mAChR (for a review see Wess, 2004). M1, M3 and M5 mAChRs are coupled to the Gαq/11 G-protein family and activate phospholipase C. These receptors are mainly located on postsynaptic elements. M1 receptor is predominant and mostly located on pyramidal cells and cortico-cortical fibers whereas, traces of M3 receptor are found in V1. On the other hand M2 and M4 receptors are coupled to α subunits of Gi/o and inhibit adenylate cyclase activity and voltage-sensitive calcium channels (Caulfield and Birdsall, 1998). These receptors also activate MAPK that regulates synaptic plasticity (Roberson et al., 1999). M2 are often found on presynaptic cholinergic (as autoreceptors) and GABAergic terminals and interneurons, where they induce direct modulatory effects as shown by in vitro studies (Caulfield and Birdsall, 1998; McCormick and Prince, 1985; Salgado et al., 2007). M4 is quite rare in V1. Muscarinic disinhibition of cortical circuits through decreased GABAergic drive (Lawrence, 2008; Zinke et al., 2006) changes the excitatory/inhibitory balance necessary for cortical plasticity. mAChRs are also involved in long-term potentiation (LTP) and depression (LTD)

* Corresponding author at: Laboratoire de Neurobiologie de la Cognition Visuelle, École d'optométrie, Université de Montréal, CP 6128, succ. Centre-ville, Montréal, Québec, H3C 3J7, Canada. Fax: +1 514 343 2382.

http://dx.doi.org/10.1016/j.neuroimage.2014.05.016
1053-8119/

mechanisms in V1 (Dringenberg et al., 2007; Kang and Vaucher, 2009; Origlia et al., 2006), which contributes to the learning and memory processes in young and adult rats.

In the present study, single or double mAChR knockout (KO) mice (M1-KO, M1/M3-KO and M2/M4-KO) were used to explore the contribution of mAChRs to the visual cortex organization using optical imaging of intrinsic signals (OIS) technique. OIS has been widely used to visualize topographic maps such as orientation (Grinvald et al., 1986; Ts'o et al., 1990), ocular dominance (Ts'o et al., 1990) or retinotopy maps in the visual system of various species, including mice (Drager, 1975; Kalatsky and Stryker, 2003; Schuett et al., 2002). The immunohistochemistry analysis was performed to associate the anatomical features to functional properties assessed with OIS.

Materials and methods

Animal preparation

All procedures were carried out in accordance with the guidelines of the Canadian Council for the Protection of Animals and were accepted by the Ethics Committee of the Université de Montréal. A total of 38 male mice (6–9 weeks) were used in this study, distributed over five groups: M1/M3-KO (M_1M_3 −/−) (n = 10), M1-KO (M_1 −/−) (n = 7), M2/M4-KO (M_2M_4 −/−) (n = 8) and their respective genetic controls, 129SvEv × CF1 (WT control mice, n = 6) for M1/M3-KO and M1-KO, and C57BL/6J (n = 7) for M2/M4-KO mice. All the strains were backcrossed for at least 10 generations (Duttaroy et al., 2002). An additional set of animals for each group (n = 4/group) was used for immunocytochemical examination of the cholinergic innervation of V1. All mAChR KO mice were kindly provided by Dr. Jurgen Wess (NIH, Bethesda, USA). The animals were maintained in a 12 h light/dark normal daylight cycle with ad libitum access to food and water. Before OIS imaging, the mice were anesthetized using urethane (1.25 g/kg, i.p.). Throughout the experiment, depth of anesthesia was periodically tested using the paw retirement reflex (10% of the induction dose was given additionally if needed). A tracheotomy was performed and the animal was placed in a stereotaxic frame. A flow of O_2/N_2O mixture was placed directly in front of the tracheal tube. In addition, xylocaine (0.2%, AstraZeneca, Mississauga, Ontario) was injected locally at every incision point. The eyes were hydrated every 10–20 min with ocular drops (Blink, Abbott, Illinois, USA). Core body temperature was maintained at 37 °C using a feedback controlled heating pad (Harvard Apparatus, Saint-Laurent, Québec) and electrocardiogram (FHC, Bowdoin, ME, USA) was continuously monitored with subdermal electrodes. The visual cortex was imaged through the skull: an imaging chamber was placed over both hemispheres, glued on the skull, filled with agarose (1%) and sealed with a coverslip (Figs. 1A, B). At the end of the experiment, mice were perfused with 45–60 mL of 4% paraformaldehyde in 0.1 M phosphate buffer sodium at room temperature. Brains were then dissected and kept for immunohistochemistry.

Optical imaging

Stimulation

Visual stimulation was provided using a custom made software (STIMPlus) and presented by an LCD projector on a screen placed at a distance of 20 cm in front of the mouse eyes (subtending 150 × 135° of visual angle). To assess visuotopy and characterize maps and

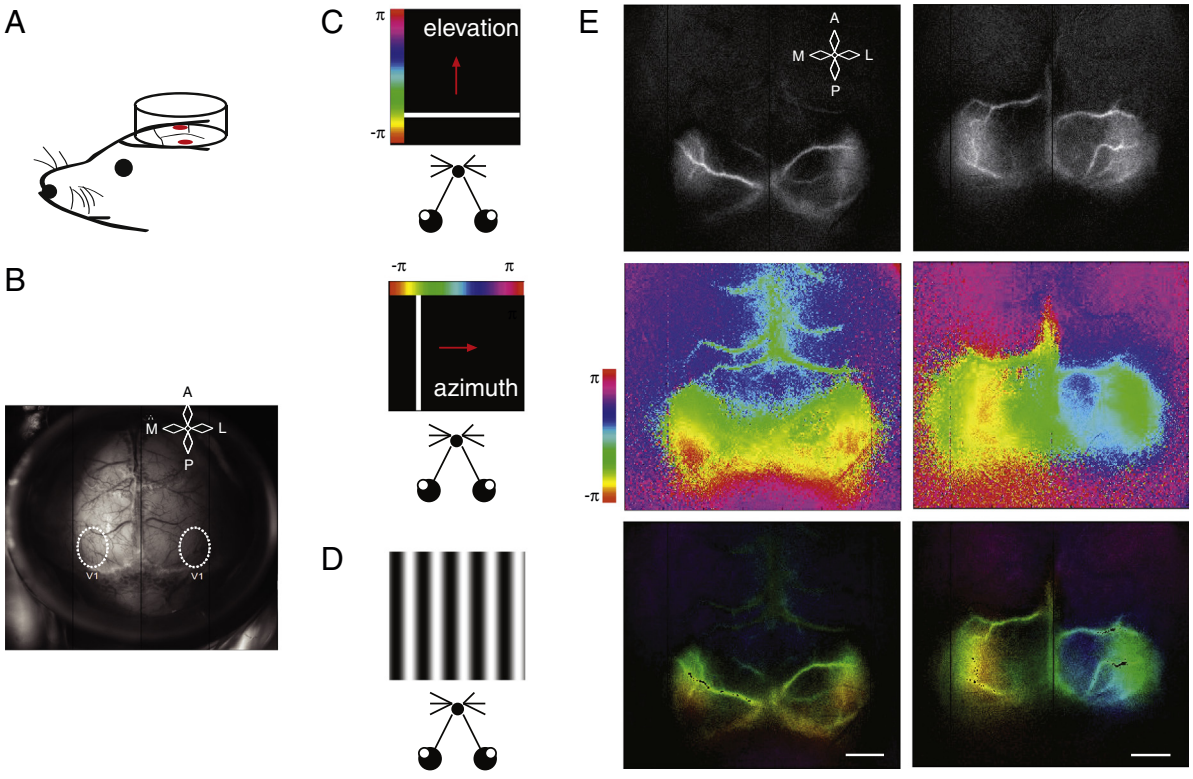

Fig. 1. Topographic maps and functional organization of V1 using optical intrinsic signal imaging. A. For OIS assessment, an imaging chamber is placed over the skull of the animal. B. Vasculature pattern of the brain as assessed with 545 nm illumination. V1 is represented (ovals). C. Schematic representation of continuous paradigm of visual stimulation: a bar was shifted along elevation and azimuth at 0.1 or 0.2 Hz. The pseudocolor scale represents the degree of visual field stimulated (π to 2π). D. Schematic representation of episodic full-field sine wave grating stimulation. The screen was placed in front of the animal. E. Representative maps obtained using OIS. Top panel: "neuronal activation" map along elevation (left) and azimuth (right). Middle panel: color-coded "visual field position" map along elevation (left) and azimuth (right). Bottom panel: "retinotopic" map along elevation (left) and azimuth (right). The retinotopic map is the combination of the gray scale color coded responses magnitude map (top) and color-coded phase map (middle). See text for details. Scale bar = 50 pixels. A: Anterior, P: Posterior, M: Medial, L: Lateral.

connectivity in V1, a continuous stimulation paradigm (Kalatsky and Stryker, 2003; Vanni et al., 2010) was used, where 2° thick light bars were periodically shifted horizontally (to obtain elevation maps) or vertically (to obtain azimuth maps) over a dark background at a frequency of 0.1 Hz (Fig. 1C). These relative retinotopic maps were used to assess several structural and functional parameters within V1 but were not used here to delineate visual areas (such as in fMRI studies) or evaluate precise positions of receptive field (such as in traditional electrophysiological studies). To examine the functional properties of V1 neurons, episodic full-field sine wave grating stimuli (four directions: 0, 90, 180, 270°) were presented during 2 s and spaced by a blank presentation lasting 18 s intervals (mean luminance 75 cd/m^2) (Fig. 1D). The amplitude of the hemodynamic responses was measured as a function of contrast and spatial frequency selectivity. Five contrasts (6%, 12%, 25%, 50% and 100%) and four spatial frequencies (0.005, 0.01, 0.02 and 0.04 cycle per degree (cpd)) were used to determine contrast sensitivity and spatial frequency selectivity, respectively.

Image acquisition

The cortex was illuminated at 545 nm to adjust the focus of the camera and at 630 nm to record the intrinsic signals. Optical images were recorded using a 12-bit CCD camera (1M60, Dalsa, Colorado Springs, USA) driven by the Imager 3001 system (Optical Imaging Inc.©) and fitted with a macroscopic lens (Nikon, AF Micro Nikon, 60 mm, 1:2:8D). Frames of 512 × 512 pixels were acquired at a rate of 4 Hz, giving a spatial resolution of 28 μm/pixel. The acquisition was sustained for 10 min during the continuous stimulation paradigm. During episodic stimulation, frames were acquired for 20 s for every contrast and spatial frequency tested. An average of 10 repetitions was used to obtain a good signal to noise ratio.

Data analysis

OIS result from a complex interplay between neuronal activity and vascular response (Frostig et al., 1990; Hillman et al., 2007; Vanzetta and Grinvald, 2008). The reflectance of the intrinsic signals is produced by a modification of the oxy/deoxy-hemoglobin ratio, relative to pure neuronal activity (oxygen consumption) or changes in blood volume or blood flow to adjust for the metabolic need of the neurons (hemodynamic response). The visual parameters analyzed from the OIS in the present study are thus representative of local activity of neurons rather than pure vascular response, in agreement with previous studies (Vanzetta and Grinvald, 1999). It is also assumed here that mAChR deletion does not change the OIS signal with regard to possible blood flow effects. Although vasodilatory effects of mAChRs are well known (Hamel, 2004), it is unlikely that mAChR deletion does change the hemodynamic response to visual stimulation in the present study for the following reasons. First, predominantly M5 but not M1, M2, M3 or M4 mAChRs contributes to the cholinergic-induced blood flow changes in the cortex (Elhusseiny et al., 1999; Hamel, 2004; Wess, 2004; Yamada et al., 2001) and M5 mAChR was not deleted in the group of mice examined here. Second, the contribution of acetylcholine on hemodynamic response to sensory stimulation has been shown to be minor compared to effects of glutamatergic or GABAergic local cortical neurons (Lecrux et al., 2011). Moreover, the hemodynamic response obtained with episodic stimulation (Figs. 4E, F) is composed of two phases, an initial dip where the concentration of deoxyhemoglobin increases – representative of oxygen consumption – followed by a positive peak – representative of an increase of the oxyhemoglobin, secondary to an increase of blood volume/blood flow (Vanzetta and Grinvald, 2008). In our study, the contrast sensitivity and optimal spatial frequency were established from the amplitude of the negative peak of the first part of the hemodynamic response, and is thus related to neuronal activity rather than blood volume changes. If mAChR deletion did affect the hemodynamic response, it would not have been considered since the second part of the hemodynamic response was not included in the analysis.

OIS data were analyzed with MATLAB (MathWorks, Nattick, MA). For each pixel of the cortex, a Fourier transform was applied on temporal signals collected during continuous stimulation (Kalatsky and Stryker, 2003). Fourier phase and amplitude were generated for each frequency and used to map the retinotopy and realize quantification. The amplitude of neuronal activity was used to generate the "neuronal activation" map (Fig. 1E, upper panel). In parallel, the phase at the stimulus frequency was related to the delay to activate the receptive field and was associated to the relative retinotopic position (Fig. 1E, middle panel). The "retinotopic" map (Fig. 1E, lower panel) was obtained by multiplying the amplitude and phase maps. Regions of interest (ROI) located in the occipital cortex were manually delineated in the activation maps for each hemisphere. The area of V1 was calculated from the ROI borders. The shape of the ROI was fitted to an ellipse with MATLAB and the ratio of length of the two main axes of the ellipse determined (height/width) was calculated to measure the "ovality index" (Fig. 2A). The ratio of the number of the phases detected in the retinotopic maps over 2π (i.e. the range of the phases displayed) was

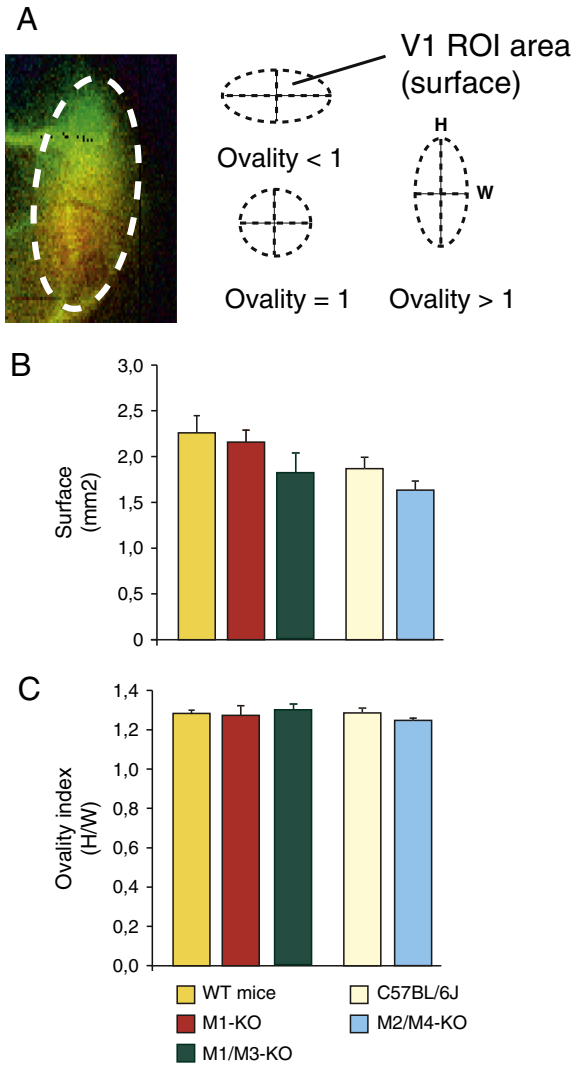

Fig. 2. Surface and shape of the visual cortex in mAChR-KO and wild type mice. A. Left. Responsive visual area fitted with an ellipse. Right. Graphical representation of different values of the ovality index of V1. The two main axes were measured on the delimited V1. The ovality index was calculated from the ratio height/width (H/W). B. Histograms of the surface of V1 (mm^2) in the different groups. The surface was not statistically changed between the mAChR-KO compared to their wild type mice. C. Ovality index measurement. No statistical changes were seen between the mAChR-KO compared to their controls. Error bars represent ± s.e.m.

used to estimate the "apparent visual field", i.e. the proportion of the activated visual field represented in V1. The difference between the phase of each pixel and its surrounding pixels was calculated on the phase map to evaluate the "scatter index" (Fig. 3A). Being related only to the delay and frequency of the response rather than its amplitude, this parameter is independent of the amplitude of the signal thus independent of the intensity of blood volume changes, and rather it gives an estimate of the retinotopy accuracy (Cang et al., 2005a, 2008). Accordingly to the method presented by Vanni et al. (2010), Fourier amplitude at the stimulus frequency and second harmonic was used to evaluate the population receptive field (pRF) size of the underlying neurons (neurons within a ROI respond to a range of visual field locations and the region of the visual space that stimulates this local neuronal activity is called pRF). Briefly, when each bar travels into a pRF the neuronal activity increases. When the spatial extent of pRF is large, the duration of the neuronal activity should be long while for smaller pRF, a narrower temporal response is expected. Thus, broader temporal response generated for large pRF should produce a more sinus waveform than small pRF which should be associated to a "sharper" waveform. Therefore, because sharper waveform is associated with higher harmonics amplitude, the ratio between the second to the first harmonic was used as an inverse measure of the pRF size.

The hemodynamic responses obtained during episodic stimulation were used for the functional analysis of the neuron features. The contrast and spatial frequency tuning curves for each pixel of V1 were established from the amplitude of the negative peak of the hemodynamic response (Figs. 4E, F). The spatial frequency producing the strongest hemodynamic response was calculated for each pixel. The results of each trial at all orientations were pooled and the average value of spatial frequency of all pixels of V1 was defined as the optimal spatial frequency. The curves of amplitude as a function of the contrast were fitted with a Naka-Rushton function (Carandini and Sengpiel, 2004) to determine the contrast evoking 50% of the maximum response.

Immunohistochemistry

Intracardiac perfusion of 4% freshly prepared paraformaldehyde was performed under deep anesthesia (urethane, 1.25 g/kg, i.p.). Fixed brains were collected, post-fixed for 2 h in the same fixative, and stored in 0.1 M phosphate buffered saline (PBS, pH 7.4) overnight. Brains were sliced into 35-μm sections using a vibratome (VT1000, Leica microsystems) at the level of the visual cortex/superior colliculus (−3.52 mm from Bregma). Brain sections were collected and serially stored for proper antero-posterior identification. Sections were pre-incubated for 20 min at room temperature (RT) in PBS, (0.1 M, pH 7.4) containing 0.3% hydrogen peroxide, followed by 30 min in PBS containing 0.25% Triton X-100 and 1.5% donkey serum (Jackson ImmunoResearch, Westgrove, PN, USA). Sections were incubated overnight at RT with goat anti-choline acetyltransferase (ChAT) primary antibody (1:200, Chemicon, EMD Millipore, Billerica, MA, USA) in PBS-Triton, followed by 2 h incubation in secondary antibody (1:200, donkey-anti-goat, Jackson ImmunoResearch, Westgrove, PN, USA). Visualization was achieved by 1 h in the avidin–biotin complex (ABC Elite kit, Vector Laboratories, Burlingame, CA, USA) followed by peroxidase-substrate-kit Vector SG (Vector Laboratories) for a standardized period of 5 min. Sections were then mounted onto slides, dehydrated and sealed with coverslips.

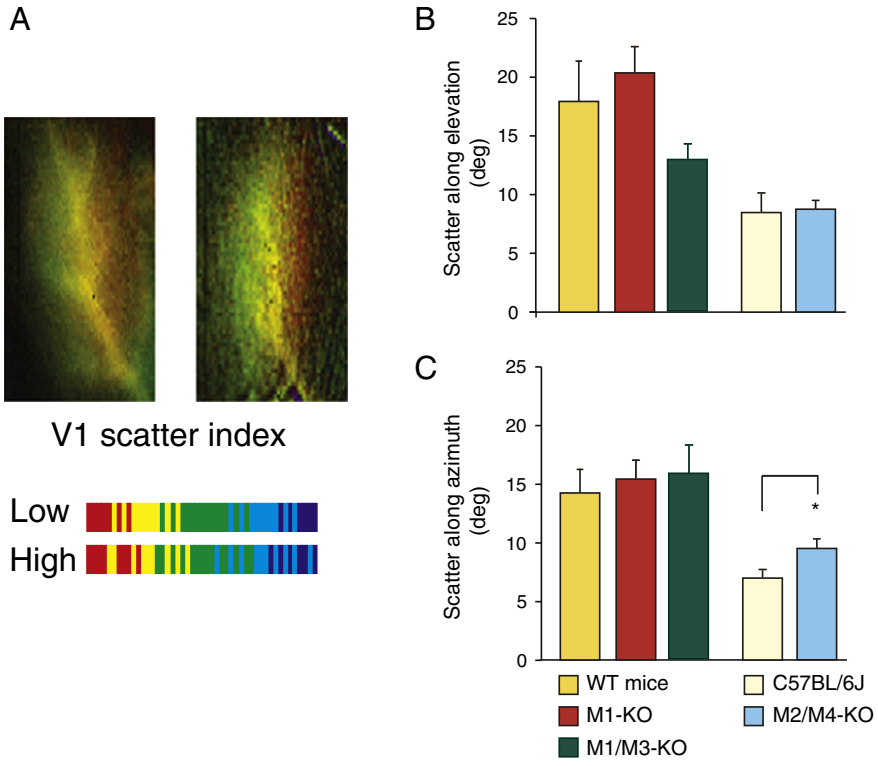

Fig. 3. Evaluation of the scatter index. A. Representative visual field position map of C57BL/6J (left) and M2/M4-KO (right) showing the increased scatter in V1 of M2/M4-KO, which corresponds to a larger overlap between LGN projections. Bottom: representation of the overlap of the color-coded projections of the LGN of a low scatter index vs. a high scatter index. B. Histograms of the scatter index values of V1 in the different groups (deg) along the elevation axis. No statistical changes occurred between M1/M3-KO, M1-KO or M2/M4-KO mice compared to their wild type mice. C. Histograms of the scatter index of V1 along the azimuth axis. M2/M4-KO mice showed an increase of the scatter index compared to their wild type but no statistical changes occurred between M1/M3-KO or M1-KO compared to their wild type. Error bars represent ± s.e.m.

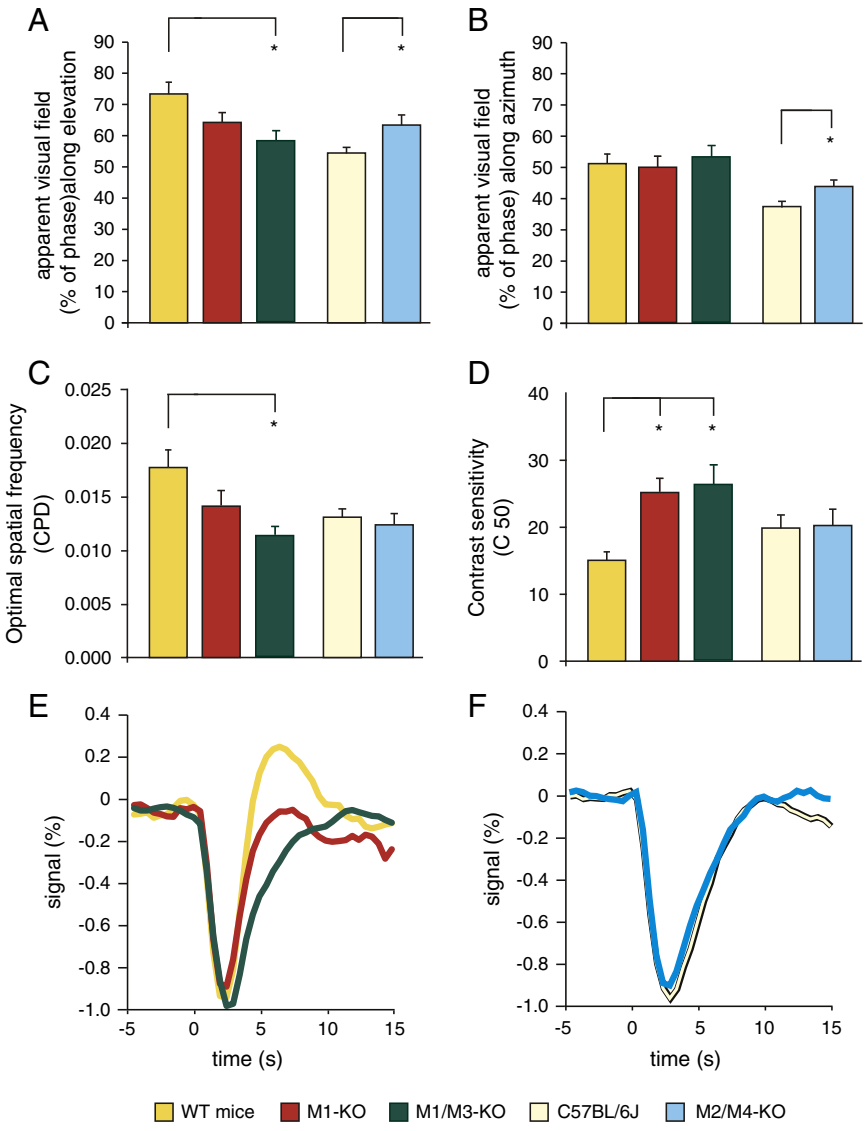

Fig. 4. Sensitive properties of V1 and apparent visual field. A. Graphical representation of the apparent visual field of V1 in the different groups along elevation. M1/M3-KO and M2/M4-KO mice showed respectively a decreased and an increase of the apparent visual field compared to their control. B. Representation of the apparent visual field of V1 in the different groups along azimuth. M2/M4-KO mice showed an increased apparent visual field compared to their controls. C. Measurement of the optimal spatial frequency. For M1/M3-KO mice, the optimal spatial frequency was decreased compared to their wild-types. No statistical changes are observed between M2/M4-KO mice and their wild-types. D. Measurement of the contrast sensitivity (C50). Both M1/M3-KO and M1-KO mice showed an increased contrast evoking 50% of the maximal response. No statistical changes were seen between M2/M4-KO mice compared to their wild-types. E. Representation of averaged the hemodynamic responses of V1 for M1-KO, M1/M3-KO and their controls. F. Representation of the hemodynamic responses of V1 between M2/M4-KO mice and their controls. Error bars represent ± s.e.m.

Stereological estimation of fiber density and varicosity

Stereological sampling and analysis was carried out in blind experimental conditions. Analysis was performed on 5 sections covering the extent of the primary visual cortex (−4.04 to −2.18 from Bregma). V1 was anatomically delineated at low magnification (10×) with reference to mouse brain atlas (Paxinos and Franklin, 2012). Stereological counting of varicosities and fibers was performed at 100× magnification (Leica HCX PL Fluotar oil-immersion objective) using Leica DMR microscope with StereoInvestigator software (v9.13, MicroBrightField, Williston, VT) and a computer driven motorized stage. A sampling grid (250 × 210) was used. V1 was systematically sampled with a minimum average of 100 optical dissectors measuring 5 × 5 × 5 μm^3. Guard zones were applied in all cases. The hemisphere spaceball probe was used to estimate fiber density in V1 (Mouton et al., 2002). Optical-fractionator systematic sampling design was used to estimate the total number of varicosities (West et al., 1991). An average of 169 varicosities per animal was counted at random over the whole extent cortical layers. The estimation of varicosities density was calculated by the sum of the counted varicosities in the dissectors multiplied by the section sampling fraction multiplied by the area sampling fraction multiplied by the thickness-sampling fraction. A coefficient of error (CE) of the estimation is used to assess the precision of the sampling (Gundersen et al., 1999). Each of the measured mice CE was ≤0.1 that indicates adequate stereological sampling parameters (Mouton et al., 2002; West et al., 1991). Ratios of puncta density/fiber density were calculated for each animal and then averaged together (Table 1).

Statistical analysis

For all the imaging parameters, the groups WT mice, M1/M3-KO and M1-KO were compared using one-way ANOVA. Post-hoc test was carried out using LSD correction. C57BL/6J and M2/M4-KO were compared using Student's *t*-test. C57BL/6J and 129SvEv × CF1 (named WT mice)

Table 1
Cholinergic fibers and varicosity density in the primary visual cortex of mAChR-KO and wild type mice.

	Total punctae ($x10^5$)	Total fibres (m)	Puncta density ($10^6/mm^3$)	Fibre density (m/mm^3)	Ratio Puncta/fibre
WT mice	4.85 ± 1.74	1.50 ± 0.26*	3.22 ± 0.85	10.12 ± 1.85**	0.32 ± 0.07
M1/M3-KO	5.84 ± 1.32	1.23 ± 0.16*	3.37 ± 0.75	7.10 ± 0.37**	0.49 ± 0.14
M1-KO	6.58 ± 2.32	1.63 ± 0.24*	3.37 ± 0.84	8.60 ± 1.85**	0.41 ± 0.16
C57BL6	5.01 ± 1.41	1.30 ± 0.34	2.69 ± 0.52	7.07 ± 1.44	0.39 ± 0.06
M2/M4-KO	4.66 ± 1.24	1.25 ± 0.13	2.54 ± 0.63	6.83 ± 0.64	0.38 ± 0.11

Values are mean ± SD. The first two columns (light gray) represent an estimation of the number of puncta and fiber length in the entire primary visual cortex ('total values' as stereological data). The two next columns (medium gray) represent the number of puncta and fiber length corrected for the volume of V1 ('density values'). The last column (dark gray) is the ratio of the puncta over the fiber length calculated for each animal, i.e. the distribution of the puncta along the fiber. See text for details.
*Kruskal–Wallis K = 6.260, p = 0.044.
**Kruskal–Wallis K = 0.240, p = 0.027.

were compared using Student's *t*-test. For immunohistochemistry analysis, groups WT mice, M1/M3-KO and M1-KO were compared using Kruskall–Wallis test. C57BL/6J and M2/M4-KO were compared using Mann–Whitney test. Statistical analyses were performed using SPSS 17.0 (SPSS Inc., Chicago, IL, USA) with a significance level of $p < 0.05$.

Results

Visual parameter differences between strains of mice

Two strains of mice were used in this study, i.e. C57BL/6J and 129SvEv × CF1 (WT mice). The different mice did not show any behavioral deficits or major cognitive impairments, excluding hyperlocomotion in M1-KO mice (Wess, 2004). There was a significant lower optimal spatial frequency (*t*-test, p = 0.0028, Fig. 2B) and extent of the apparent visual field along azimuth (*t*-test, p = 0.001) and elevation (*t*-test, p = 0.003, Fig. 4B) in the C57BL/6J compared to 129SvEv × CF1 WT mice. The scatter index was however significantly smaller along azimuth (*t*-test, p = 0.005, Fig. 3B) and elevation (*t*-test, p = 0.026) in the C57BL/6J compared to 129SvEv × CF1 WT mice. The other parameters measured in the present study were not significantly different between the two strains. These findings support a difference of visual acuity between strains. This agrees with previous studies showing that the visual acuity threshold is higher in C57BL/6J than in 129 strains (at least the 129S1/SV1MJ substrain) (0.375 vs 0.245 cpd, respectively) (Wong and Brown, 2006) and that their speed to perform a discrimination task in the visual water maze is different. The pattern and stimuli detection threshold is however identical between C57BL/6J and 129S1/SV1MJ (Wong and Brown, 2006). The aim of this study was not to determine the more adequate strain of mice for vision research. We rather performed a statistical analysis of the relative changes of the parameters within each strain related to the specific effect of mAChR subtype deletion.

Contribution of the muscarinic receptors to the retinotopic maps in V1

The effect of mAChR deletion on V1 retinotopic maps was first analyzed by measuring the cortical surface and shape allocated for the response to the visual stimulation following the continuous visual stimulation paradigm (Fig. 1 and see Materials and methods section for details). The area of V1 was not statistically different between WT control mice, M1/M3-KO or M1-KO (ANOVA, $F_{1.505} = 0.246$) nor between C57BL/6J and M2/M4-KO (*t*-test, p = 0.157) (Fig. 2B). The ovality index (Figs. 2A, C and see Materials and methods section for details) was not statistically different between WT mice, M1/M3-KO and M1-KO (ANOVA, $F_{0.248} = 0.783$) nor between C57BL/6J and M2/M4-KO (*t*-test, p = 0.114). Therefore, the area and shape of V1 were not affected by mAChR deletion. Moreover, the index of the scatter – an index of architectonic organization of the cortex – was evaluated to assess the accuracy of the retinotopic map (Fig. 3A and see Materials and methods section for details). No change of this index was found along azimuth (ANOVA, $F_{0.155} = 0.858$, Fig. 3C) nor elevation (ANOVA, $F_{1.792} = 0.194$, Fig. 3B) between WT mice, M1/M3-KO and M1-KO. However, an increase of the scatter index along azimuth (*t*-test, p = 0.041, Fig. 3C) but not along elevation (p = 0.859, Fig. 3B) was observed in M2/M4-KO mice compared to C57BL/6J. This suggests that the retino-geniculo-cortical projection organization or the neuronal connectivity within V1 was affected by M2/M4 receptors but not M1 or M3 mAChRs.

Contribution of the muscarinic receptors to the apparent visual field

The organization of V1 was also characterized by quantifying the percentage of visual field encoded on the visual cortex over the extent of the stimulated visual field. The apparent visual field (the proportion of the visual field represented in V1) was shrunken along elevation in M1-KO ($F_{3.382} = 0.055$, ANOVA, post-hoc LSD, p = 0.033) mice compared to WT mice but not in M1/M3-KO (Fig. 4A). Nevertheless, it was not altered along azimuth (ANOVA, $F_{0.270} = 0.766$) between WT mice, M1/M3-KO and M1-KO (Fig. 4B). The apparent visual field was enlarged along azimuth (Fig. 4A) as well as along elevation (Fig. 4B) in M2/M4-KO mice compared to C57BL/6J (*t*-test, p = 0.031 and *t*-test, p = 0.025, respectively). Taken together, these results suggest an opposite effect of M1 vs. M2/M4 receptor on the cortical coverage of the visual field integration.

Contribution of the muscarinic receptors to the spatial RF properties of V1 neurons

The optimal spatial frequency and contrast function were assessed for the different groups of mice by analysis of the amplitude of the signal obtained by episodic stimulation. The optimal spatial frequency was significantly reduced in M1/M3-KO mice compared to WT mice (WT: 0.018 ± 0.002 cpd, M1/M3-KO: 0.011 ± 0.001 cpd, ANOVA, $F_{5.574} = 0.013$, p = 0.040) whereas no reduction was observed in M1-KO mice (M1-KO: 0.014 ± 0.002 cpd, Fig. 4C), suggesting a specific involvement of M3 in high spatial frequency tuning of cells in V1. No statistical difference was observed in the optimal spatial frequency between C57BL/6J and M2/M4-KO mice (M2/M4-KO: 0.012 ± 0.001 cpd, C57BL/6J: 0.013 ± 0.001 cpd, *t*-test, p = 0.640, Fig. 4C). The C50, which corresponds to the contrast evoking 50% of the maximal response, was significantly higher in M1/M3-KO (ANOVA, $F_{7.429} = 0.006$, p = 0.003) and M1-KO (p = 0.009) indicating a reduced contrast sensitivity in those animals compared to WT mice (Fig. 4D). This suggests an influence of M1 and possibly M3 mAChRs in contrast discrimination. C50 was not changed between C57BL/6J and M2/M4-KO (*t*-test, p = 0.900). Hemodynamic responses obtained at maximal contrast are represented in Figs. 4E (WT, M1/M3-KO and M1-KO) and F (C57BL/6J and M2/M4-KO). An index of the size of pRFs of V1 population was assessed by calculating the ratio of the magnitude of the second over the first harmonics of the Fourier transform of the signal (Fig. 5A and see Materials and methods section for details) obtained with the continuous stimulation paradigm. In M1-KO mice, the ratio was smaller along azimuth (ANOVA, $F_{4.191} = 0.031$, p = 0.015) and elevation (ANOVA, $F_{3.565} = 0.048$, p = 0.024) was compared to WT mice (Figs. 5B, C). The ratio was decreased in M1/M3-KO along azimuth (ANOVA, $F_{4.191} = 0.031$, p = 0.032) but not along elevation (ANOVA, p = 0.752) compared to WT mice. The ratio being inversely proportional to pRF, the apparent pRF size was increased in these mice. M3 mAChR possibly compensates for a change of the pRF along elevation. This is coherent with the shift to low spatial frequency observed in M1/M3-KO mice. No statistical differences were found between C57BL/6J and M2/M4-KO along azimuth (*t*-test, p = 0.795) nor elevation (*t*-test, p = 0.622). This

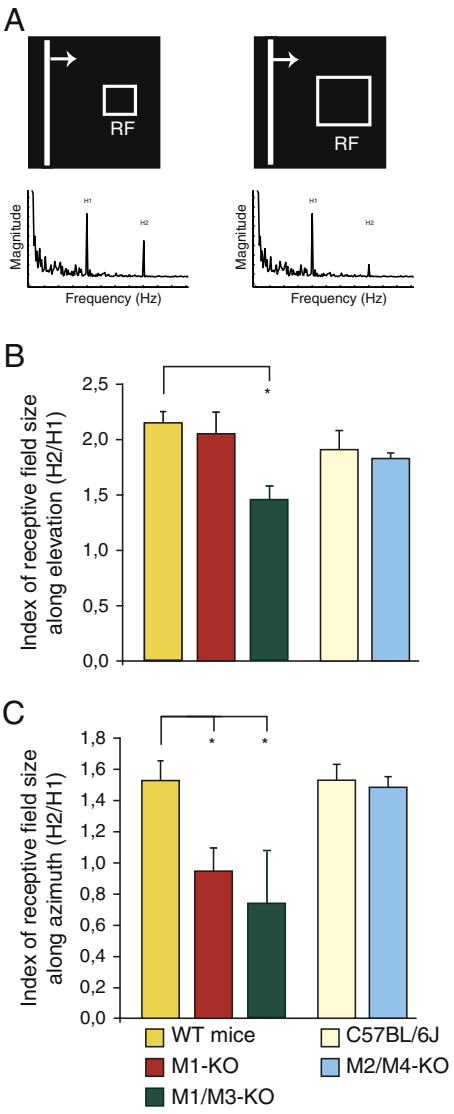

Fig. 5. Population receptive field index of mAChR-KO and wild type mice. A. Schematic representation of the population receptive field. Fourier transform of a visual response following a 10 min continuous stimulation of a drifting bar where the first (H1) and second (H2) harmonics are visible. The index of receptive field is the measure of the ratio of the second over the first harmonic of the signal. It is inversely proportional to the size of pRF (see text for details). B. Graphic representation of the index of the pRF size along elevation in the different groups. The ratio H2/H1 is decreased between the M1/M3-KO compared to their wild type mice. C. Graphic representation of the index of the pRF size along azimuth. The ratio H2/H1 is decreased in both M1-KO and M1/M3-KO compared to their wild types. This suggests that the size of pRF is increased in M1-KO and M1/M3-KO. Error bars represent ± s.e.m.

suggests that M2/M4 mAChRs do not affect spatial properties of pRF structure of V1 neurons; which is consistent with the absence of change in the spatial frequency and contrast sensitivity.

Contribution of the muscarinic receptors to the cholinergic innervation of V1

The analysis of the cholinergic innervation of V1 in the different groups of mice was performed to determine possible changes induced by mAChR deficit on cholinergic input to V1. As already reported, ChAT-stained fibers appeared as fine lines (axons) of varying lengths and thicknesses endowed with varicosities — ellipsoid or round shaped dark swellings (puncta) present along the fibers (Fig. 6). The cholinergic innervation was more dense in the layer IV compared to layers I or VI. The total length of fibers over V1 and density of fibers as well as the total number of puncta over V1 and density of puncta (Table 1) hinted the level of local volumetric transmission and neuronal interactions (Mechawar et al., 2000). The fiber density as well as total length of fiber was significantly ($K = 0.240$, $p = 0.027$ and $K = 6.260$, $p = 0.044$, respectively) changed between M1, M1/M3 KO and their WT, with an apparent reduction of the fiber density in M1/M3 KO. This suggests that deletion of the two excitatory mAChRs leads to a slight reduction of cholinergic innervation of V1. However, the density of puncta as an absolute value or related to the fiber density was not changed between M1, M1/M3 KO and their WT counterparts ($K = 0.240$, $p = 0.887$ and $K = 2.060$, $p = 0.357$, respectively). No significant differences were observed in other measurements between M2/M4 KO and WT (fiber length: $U = 15$, $p = 0.602$; fiber density: $U = 13$, $p = 0.917$; puncta number: $U = 13$, $p = 0.917$; puncta density $U = 14$, $p = 0.754$). The comparison of the puncta density over fiber density ratios showed no significant difference (Table 1, $K = 3.140$, $p = 0.208$). Given the volume transmission mode of the cholinergic system, one may propose that the reduction of fiber density in M1 and M1/M3-KO is indicative of a reduction of the extent of the influence of the cholinergic fibers on different neuronal elements of the neuropil. However, since the limitating parameter of ACh efficacy is the number of puncta, which release ACh, along the axons (Zhang et al., 2011) and that puncta density and distribution along the fiber was not reduced in mAChR KO mice, it is likely that the influence of the cholinergic fibers on V1 in mAChRs-KO and WT mice is equivalent. This suggests that the cholinergic input of V1 was barely affected by the absence of mAChR.

Discussion

Our results indicate that the subtypes of mAChRs play distinct roles in the intrinsic organization of V1 and selective properties of V1 neurons, but not in the size of the area dedicated to primary visual processing. M1, M2 and M4 mAChRs influence the representation of the peripheral visual field with opposite effects. M2 and M4 mAChRs are involved in the smoothness of the retinotopic organization whereas, M1 and M3 modulate the size of the pRFs – as estimated over an ensemble of neurons – and fine tuning of spatial frequency and contrast properties of neurons. All these effects suggest a strong involvement of mAChRs in the detectability of visual stimuli, an influence of the mAChR deletion in the maturation of V1 and, probably, an adaptation or compensation of the neural tissue lacking mAChRs during development or maturation. Finally, these functional changes are not correlated with changes in the anatomical features of the cholinergic innervation of V1.

Muscarinic receptors influence cortical representation of the visual field

In the present study, surface and shape of V1 maps were not affected by mAChR deletion thus, the portion of the cortex devoted to the representation of the visual world was preserved. The retinotopic maps were considered as V1 maps assuming that only V1 was activated — V2 map would have been observed as a mirror image of V1 activation immediately lateral to V1 (Kalatsky, 2009) which was not detected in the present study. However, the possibility that neuronal activity could be really low at the edge of V1 and then not detected by the indirect measurement has to be considered as a possibility of underestimation of the size and shape of V1. Although the size and shape of V1 were not changed among the different groups, the extent of the visual field represented in V1 was decreased in M1-KO along elevation and increased in M2/M4-KO along elevation and azimuth. The projections from the retinal ganglion cells are formed along anteroposterior and mediolateral axes and differences between the representations of the visual field along these two axes in V1 have already been reported in mutant mice (Cang et al., 2008). The mAChR deletion-induced changes observed in the present study do not dramatically alter the representation of the visual field and correspond to an increase in peripheral vision of approximately 10%. By contradistinction, some mutations as the

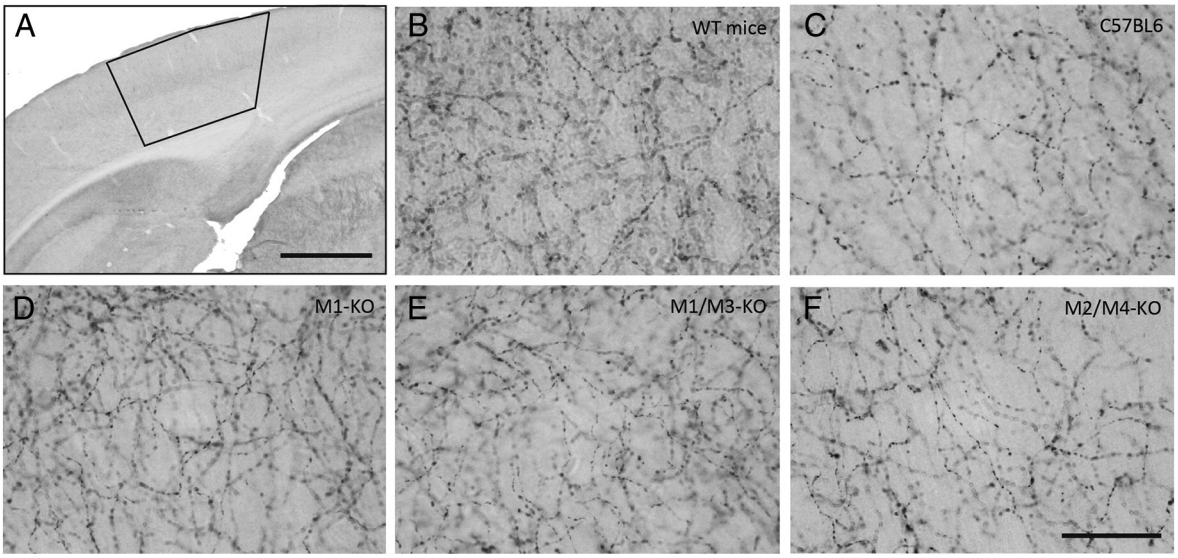

Fig. 6. Microphotographs of cholinergic fibers and varicosities in V1 of the different mice. A. 10× photograph of the selected region encompassing V1M and V1B. Anteriority −3.80 mm from Bregma. B–F. Representative ChAT-immunostained microphotographs of layer IV taken at 100×. The cholinergic pattern of innervation as well as the morphology and quantity of cholinergic fibers and varicosities are visible. B. WT mice group. C. C57BL/6J group. D. M1-KO group. E. M1/M3-KO group. F. M2/M3-KO group. Scale bar = 300 μm (A) 30 μm (F).

ephrin deletion have been shown to completely disorganize the retinotopic map of V1 (Cang et al., 2008; Willshaw, 2006). Our findings could indicate a poor versus strong processing of the peripheral vision in M1-KO and M2/M4-KO, respectively. In wild-type animals, the peripheral vision is mostly modulated by suppression of the peripheral inputs within the cortex (Palmer and Rosa, 2006; Rosa and Tweedale, 2004), although filtering of central versus peripheral inputs might also be exerted to a certain extent at the level of the retina or geniculate body. M1 mAChRs are involved in the facilitation of thalamic inputs (Amar et al., 2010; Soma et al., 2012), thus their deletion can result in increasing the suppression of thalamic inputs involved in peripheral vision in the ventrodorsal axis. The better peripheral vision in M2/M4-KO might result from an increase of the weight of peripheral visual stimuli processing due to M2/M4 mAChR deletion-induced dysregulation of the GABAergic inhibitory drive (see below). In WT animals, stimulation of M2 muscarinic transmission would thus reduce peripheral vision, which supports a role of ACh in focussed attention, in which central vision is prioritized. The lack of involvement of M3 mAChR in central vs. peripheral vision processing could arise from the fact that M3 is less abundant than M1 in V1 (Levey et al., 1991) and also from compensation mechanisms. When M1 is deleted, ACh seems to have more affinity for M2 and M4 than for M3 (Lazareno and Birdsall, 1995) but the deletion of a particular mAChR does not have an important impact over the expression of the other mAChRs (for review, see Wess, 2004).

Muscarinic receptors influence neuronal connectivity of V1

The principal effect of M2 and M4 mAChR deletion is an increase of the scatter dispersion of the retinotopic maps, which indicates an involvement of these receptors in the neuronal connectivity within V1 or in the retinothalamic connections. A strong scatter thus indicates a relative overlap between cortical neuron receptive field or a bad transition between the retinotopic specific population of cells and thus an imprecision of the retinotopy (Cang et al., 2008). The size of the population receptive field of V1 neurons does not appear to be changed by M2/M4 deletion, thus the imprecision of the retinotopy is likely related to changes in the synaptic contacts within intracortical circuitry. The response of a V1 neuron to a stimulus in the surround of its receptive field might be due to (1) the divergence of projections of the thalamocortical inputs, which can account for stimuli up to 2 mm away from the receptor field, (2) long-range horizontal connections within layer 2/3, via both excitatory and inhibitory cells and (3) feedback control from higher cortical areas which would mediate modulation from the far surround (Series et al., 2003). Thus, the overlap of receptive field as suggested by our results could be due to the action of the M2 or M4 mAChRs on divergent thalamocortical inputs or on intracortical horizontal connections.

Two mechanisms of action mediated by M2 or M4 mAChRs might be involved in these processes: the control of ACh release or of the GABAergic inhibitory drive. Vesicular ACh release is decreased by M2 mAChRs (Rouse et al., 1999) located on cholinergic axons (Disney et al., 2006; Mrzljak et al., 1996; Zhang et al., 2002). To the other hand M4 mAChRs generally reduce the excitatory drive through a presynaptic mechanism (Kimura and Baughman, 1997). In consequence, M2/M4 deletion most probably produces a prolonged cortical ACh release resulting in increased activation of V1 pyramidal neurons or stellate cells and increased excitatory drive. In disagreement with increased release of ACh in M2/M4-KO inducing an overlap of the RFs, high level of ACh is usually associated with (1) suppression of the spread of thalamocortical activation in rats (Kimura et al., 1999) and human (Silver et al., 2008), probably mediated by M1 mAChR on intracortical connections and (2) reduction of RFs in V1 (Roberts et al., 2005). Thus, the above-mentioned studies suggest that M2 and M4 receptors might rather be involved in the modulation of RFs through other pathways than the regulation of ACh extracellular levels. GABAergic neurons have been shown to exert a strong regulation of neuronal activity, lateral connectivity within V1 (Chattopadhyaya et al., 2007; Hagihara and Ohki, 2013; Series et al., 2003; Sillito, 1975, 1977; Yazaki-Sugiyama et al., 2009). M2 and M4 receptors have been evidenced on certain types of GABAergic neurons and terminals in V1 (Disney and Aoki, 2008; Disney et al., 2006; Levey et al., 1991) and induce the decrease of the GABA release (Erisir et al., 2001; Salgado et al., 2007) and of the inhibitory drive (Disney et al., 2006; Thiele, 2013). M2 and M4 mAChR absence in M2/M4-KO could thus increase the weight of the lateral propagation of the thalamic inputs by relief of the GABAergic inhibitory drive.

Muscarinic receptors influence function of the V1 neurons

M2 mAChR deletion had no impact on the extent of V1 neurons RFs, whereas M1 and M3 mAChR deletion caused an increase in pRF size. This is in agreement with a study showing that ACh is involved in

modification and organization of the RFs in the somatosensory cortex (Delacour et al., 1990). Moreover, the local administration of ACh or AChR agonists modifies RF properties of V1 neurons (Greuel et al., 1988). Cortical RFs are formed by precise thalamocortical projections (Buonomano and Merzenich, 1998) and are modulated by intracortical connections (Series et al., 2003). It has been demonstrated that presynaptic activation of M1 mAChR reduces inhibitory lateral connections in the visual cortex (Kimura and Baughman, 1997).

The properties of V1 neurons – contrast function and optimal spatial frequency – are altered in M1- and M1/M3-KO mice, indicating that these receptors play an important role in visual stimulus detectability. Our findings corroborate previous studies showing modulation of neuronal properties in V1 by ACh as recently reviewed (Soma et al., 2013; Thiele, 2013). Contribution of the mAChR on contrast sensitivity has been shown in adult tree shrew, where administration of a muscarinic agonist produced an increase of the contrast response (Bhattacharyya et al., 2012). Contrast adaptation has been reported in neurons of V1 (Movshon and Lennie, 1979) and stimulation of the basal forebrain produces a decrease of contrast sensitivity in V1 (Bhattacharyya et al., 2013) suggesting that contrast sensitivity changes seen in the M1/M3 mAChR KO mice could be due to mechanisms in V1 rather than other levels of the visual hierarchy. However, as the retina expresses the five subtypes of mAChRs (Gericke et al., 2011) and is strongly involved in contrast adaptation, one could not exclude that contrast adaptation could also be regulated at this first level of the visual pathway (Baccus and Meister, 2002). In V1, the reduction of the contrast sensitivity could be related to the inhibitory function of M1/M3 mAChRs in corticocortical connections and the propagation of thalamocortical inputs through lateral connections in V1 (Kimura and Baughman, 1997; Kimura et al., 1999; Soma et al., 2013). As previously mentioned, the reduction of the optimal spatial frequency in KO mice might also be due to V1 mechanisms and a larger overlap of the receptive fields, decreasing the fine discrimination of high spatial frequency stimuli. This modulation of the spatial frequency discrimination corroborates a previous study showing a contribution of the cholinergic system in visual discrimination capacity (Kang et al., 2013).

Muscarinic receptors influence development and maturation of V1

The neuromodulatory effects observed in the present study are not solely due to the acute effects of mAChR inhibition as a selective pharmacological antagonist would do, but most probably to adaptation or compensation of the neural tissue devoid of a specific mAChR subtype during embryogenesis or maturation. The establishment of V1 retinotopy – axon growth and neuronal migration – seems relatively preserved throughout the visual pathway since the volume and shape of V1 are constant in the different lines of mice. In contrast, mAChRs seem involved in fine tuning of the visual function, i.e. optimal spatial frequency and precision of the connectivity. Thalamocortical mapping occurs during the first post-natal week (Cang et al., 2005b) and refinement and pruning of thalamocortical projections mostly occur during maturation and critical period which starts at the third post-natal week and ends at the fifth one (Fagiolini et al., 1994). The pattern of the cholinergic innervation of the occipital cortex is already established at this timing (Mechawar et al., 2000) with a great density of mAChRs (Aubert et al., 1996). During this period, LTP and LTD mechanisms drive the consolidation of the most used synapses (Hensch, 2005) and are altered in mAChR KO mice (M1-KO, M1/M3-KO and M2/M4-KO) (Origlia et al., 2006). Thus, the involvement of the muscarinic modulation of the visual connectivity most probably occurs during maturation of the visual cortex, rather than during development. In support of this idea, the density of cholinergic varicosities – an index of neuronal activity (Zhang et al., 2011) – in V1 was identical among the different groups of mice suggesting that the absence of mAChRs does not induce structural changes in cholinergic innervation patterns.

Conclusion

This study demonstrates that mAChRs are mandatory for proper functioning of the visual cortex and post-natal maturation. This involvement of the mAChRs in visual neuron properties adds to the function of ACh in controlling response gain by mAChRs and in attentional or learning processes in V1. Our study suggests that M2 and M4 mAChRs influence the precision of the representation of the visual world since the visual field is increased and the scatter index is decreased. It further indicates that M1 and M3 mAChRs are involved in the basic characteristics of V1 given that the visual field, the estimated pRFs and the neuronal sensitivity are changed in M1/M3 KO mice. Thus, the present study may lead to further research on the effectiveness of cholinergic pharmacological treatment to potentiate processing of visual information in the visual cortex.

Acknowledgments

Grant sponsor: Canadian Institute for Health Research; Grant number: MOP-111003 (EV). Natural Sciences and Engineering Research Council of Canada; Grant number: 238835-2011 (EV). Natural Sciences and Engineering Research Council of Canada; Grant number: 194670 (CC). MG received financial support from the School of Optometry and FRSQ Vision Research Network. The authors are thankful to Dr Sébastien Thomas for providing expert advices for optical imaging data analysis and critical review of the paper.

References

Amar, M., Lucas-Meunier, E., Baux, G., Fossier, P., 2010. Blockade of different muscarinic receptor subtypes changes the equilibrium between excitation and inhibition in rat visual cortex. Neuroscience 169, 1610–1620.
Aubert, I., Cecyre, D., Gauthier, S., Quirion, R., 1996. Comparative ontogenic profile of cholinergic markers, including nicotinic and muscarinic receptors, in the rat brain. J. Comp. Neurol. 369, 31–55.
Baccus, S.A., Meister, M., 2002. Fast and slow contrast adaptation in retinal circuitry. Neuron 36, 909–919.
Bear, M.F., Singer, W., 1986. Modulation of visual cortical plasticity by acetylcholine and noradrenaline. Nature 320, 172–176.
Bhattacharyya, A., Biessmann, F., Veit, J., Kretz, R., Rainer, G., 2012. Functional and laminar dissociations between muscarinic and nicotinic cholinergic neuromodulation in the tree shrew primary visual cortex. Eur. J. NeuroSci. 35, 1270–1280.
Bhattacharyya, A., Veit, J., Kretz, R., Bondar, I., Rainer, G., 2013. Basal forebrain activation controls contrast sensitivity in primary visual cortex. BMC Neurosci. 14, 55.
Buonomano, D.V., Merzenich, M.M., 1998. Cortical plasticity: from synapses to maps. Annu. Rev. Neurosci. 21, 149–186.
Cang, J., Kaneko, M., Yamada, J., Woods, G., Stryker, M.P., Feldheim, D.A., 2005a. Ephrin-As guide the formation of functional maps in the visual cortex. Neuron 48, 577–589.
Cang, J., Renteria, R.C., Kaneko, M., Liu, X., Copenhagen, D.R., Stryker, M.P., 2005b. Development of precise maps in visual cortex requires patterned spontaneous activity in the retina. Neuron 48, 797–809.
Cang, J., Wang, L., Stryker, M.P., Feldheim, D.A., 2008. Roles of ephrin-As and structured activity in the development of functional maps in the superior colliculus. J. Neurosci. 28, 11015–11023.
Carandini, M., Sengpiel, F., 2004. Contrast invariance of functional maps in cat primary visual cortex. J. Vis. 4, 130–143.
Caulfield, M.P., Birdsall, N.J., 1998. International Union of Pharmacology. XVII. Classification of muscarinic acetylcholine receptors. Pharmacol. Rev. 50, 279–290.
Chattopadhyaya, B., Di Cristo, G., Wu, C.Z., Knott, G., Kuhlman, S., Fu, Y., Palmiter, R.D., Huang, Z.J., 2007. GAD67-mediated GABA synthesis and signaling regulate inhibitory synaptic innervation in the visual cortex. Neuron 54, 889–903.
Collier, B., Mitchell, J.F., 1966. The central release of acetylcholine during stimulation of the visual pathway. J. Physiol. 184, 239–254.
Delacour, J., Houcine, O., Costa, J.C., 1990. Evidence for a cholinergic mechanism of "learned" changes in the responses of barrel field neurons of the awake and undrugged rat. Neuroscience 34, 1–8.
Disney, A.A., Aoki, C., 2008. Muscarinic acetylcholine receptors in macaque V1 are most frequently expressed by parvalbumin-immunoreactive neurons. J. Comp. Neurol. 507, 1748–1762.
Disney, A.A., Domakonda, K.V., Aoki, C., 2006. Differential expression of muscarinic acetylcholine receptors across excitatory and inhibitory cells in visual cortical areas V1 and V2 of the macaque monkey. J. Comp. Neurol. 499, 49–63.
Dotigny, F., Ben Amor, A.Y., Burke, M., Vaucher, E., 2008. Neuromodulatory role of acetylcholine in visually-induced cortical activation: behavioral and neuroanatomical correlates. Neuroscience 154, 1607–1618.
Drager, U.C., 1975. Receptive fields of single cells and topography in mouse visual cortex. J. Comp. Neurol. 160, 269–290.

Dringenberg, H.C., Hamze, B., Wilson, A., Speechley, W., Kuo, M.C., 2007. Heterosynaptic facilitation of in vivo thalamocortical long-term potentiation in the adult rat visual cortex by acetylcholine. Cereb. Cortex 17, 839–848.
Duttaroy, A., Gomeza, J., Gan, J.W., Siddiqui, N., Basile, A.S., Harman, W.D., Smith, P.L., Felder, C.C., Levey, A.I., Wess, J., 2002. Evaluation of muscarinic agonist-induced analgesia in muscarinic acetylcholine receptor knockout mice. Mol. Pharmacol. 62, 1084–1093.
Elhusseiny, A., Cohen, Z., Olivier, A., Stanimirovic, D.B., Hamel, E., 1999. Functional acetylcholine muscarinic receptor subtypes in human brain microcirculation: identification and cellular localization. J. Cereb. Blood Flow Metab. 19, 794–802.
Erisir, A., Levey, A.I., Aoki, C., 2001. Muscarinic receptor M(2) in cat visual cortex: laminar distribution, relationship to gamma-aminobutyric acidergic neurons, and effect of cingulate lesions. J. Comp. Neurol. 441, 168–185.
Fagiolini, M., Pizzorusso, T., Berardi, N., Domenici, L., Maffei, L., 1994. Functional postnatal development of the rat primary visual cortex and the role of visual experience: dark rearing and monocular deprivation. Vis. Res. 34, 709–720.
Frostig, R.D., Lieke, E.E., Ts'o, D.Y., Grinvald, A., 1990. Cortical functional architecture and local coupling between neuronal activity and the microcirculation revealed by in vivo high-resolution optical imaging of intrinsic signals. Proc. Natl. Acad. Sci. U. S. A. 87, 6082–6086.
Gericke, A., Sniatecki, J.J., Goloborodko, E., Steege, A., Zavaritskaya, O., Vetter, J.M., Grus, F. H., Patzak, A., Wess, J., Pfeiffer, N., 2011. Identification of the muscarinic acetylcholine receptor subtype mediating cholinergic vasodilation in murine retinal arterioles. Invest. Ophthalmol. Vis. Sci. 52, 7479–7484.
Gil, Z., Connors, B.W., Amitai, Y., 1997. Differential regulation of neocortical synapses by neuromodulators and activity. Neuron 19, 679–686.
Greuel, J.M., Luhmann, H.J., Singer, W., 1988. Pharmacological induction of use-dependent receptive field modifications in the visual cortex. Science 242, 74–77.
Grinvald, A., Lieke, E., Frostig, R.D., Gilbert, C.D., Wiesel, T.N., 1986. Functional architecture of cortex revealed by optical imaging of intrinsic signals. Nature 324, 361–364.
Gundersen, H.J., Jensen, E.B., Kieu, K., Nielsen, J., 1999. The efficiency of systematic sampling in stereology—reconsidered. J. Microsc. 193, 199–211.
Hagihara, K.M., Ohki, K., 2013. Long-term down-regulation of GABA decreases orientation selectivity without affecting direction selectivity in mouse primary visual cortex. Front. Neural Circ. 7, 28.
Hamel, E., 2004. Cholinergic modulation of the cortical microvascular bed. Prog. Brain Res. 145, 171–178.
Hensch, T.K., 2005. Critical period mechanisms in developing visual cortex. Curr. Top. Dev. Biol. 69, 215–237.
Herrero, J.L., Roberts, M.J., Delicato, L.S., Gieselmann, M.A., Dayan, P., Thiele, A., 2008. Acetylcholine contributes through muscarinic receptors to attentional modulation in V1. Nature 454, 1110–1114.
Heynen, A.J., Bear, M.F., 2001. Long-term potentiation of thalamocortical transmission in the adult visual cortex in vivo. J. Neurosci. 21, 9801–9813.
Hillman, E.M., Devor, A., Bouchard, M.B., Dunn, A.K., Krauss, G.W., Skoch, J., Bacskai, B.J., Dale, A.M., Boas, D.A., 2007. Depth-resolved optical imaging and microscopy of vascular compartment dynamics during somatosensory stimulation. Neuroimage 35, 89–104.
Kalatsky, V.A., 2009. Fourier approach for functional imaging, In: Frostig, R.D. (Ed.), In Vivo Optical Imaging of Brain Function, 2nd edition. CRC Press, Boca Raton (FL) (Chapter 10).
Kalatsky, V.A., Stryker, M.P., 2003. New paradigm for optical imaging: temporally encoded maps of intrinsic signal. Neuron 38, 529–545.
Kang, J.I., Vaucher, E., 2009. Cholinergic pairing with visual activation results in long-term enhancement of visual evoked potentials. PLoS One 4, e5995.
Kang, J.I., Groleau, M., Dotigny, F., Giguere, H., Vaucher, E., 2013. Visual training paired with electrical stimulation of the basal forebrain improves orientation-selective visual acuity in the rat. Brain Struct. Funct. http://dx.doi.org/10.1007/s00429-013-0582-y, in press.
Kimura, F., Baughman, R.W., 1997. Distinct muscarinic receptor subtypes suppress excitatory and inhibitory synaptic responses in cortical neurons. J. Neurophysiol. 77, 709–716.
Kimura, F., Fukuda, M., Tsumoto, T., 1999. Acetylcholine suppresses the spread of excitation in the visual cortex revealed by optical recording: possible differential effect depending on the source of input. Eur. J. NeuroSci. 11, 3597–3609.
Laplante, F., Morin, Y., Quirion, R., Vaucher, E., 2005. Acetylcholine release is elicited in the visual cortex, but not in the prefrontal cortex, by patterned visual stimulation: a dual in vivo microdialysis study with functional correlates in the rat brain. Neuroscience 132, 501–510.
Lawrence, J.J., 2008. Cholinergic control of GABA release: emerging parallels between neocortex and hippocampus. Trends Neurosci. 31, 317–327.
Lazareno, S., Birdsall, N.J., 1995. Detection, quantitation, and verification of allosteric interactions of agents with labeled and unlabeled ligands at G protein-coupled receptors: interactions of strychnine and acetylcholine at muscarinic receptors. Mol. Pharmacol. 48, 362–378.
Lecrux, C., Toussay, X., Kocharyan, A., Fernandes, P., Neupane, S., Levesque, M., Plaisier, F., Shmuel, A., Cauli, B., Hamel, E., 2011. Pyramidal neurons are "neurogenic hubs" in the neurovascular coupling response to whisker stimulation. J. Neurosci. 31, 9836–9847.
Levey, A.I., Kitt, C.A., Simonds, W.F., Price, D.L., Brann, M.R., 1991. Identification and localization of muscarinic acetylcholine receptor proteins in brain with subtype-specific antibodies. J. Neurosci. 11, 3218–3226.
McCormick, D.A., Prince, D.A., 1985. Two types of muscarinic response to acetylcholine in mammalian cortical neurons. Proc. Natl. Acad. Sci. U. S. A. 82, 6344–6348.
Mechawar, N., Cozzari, C., Descarries, L., 2000. Cholinergic innervation in adult rat cerebral cortex: a quantitative immunocytochemical description. J. Comp. Neurol. 428, 305–318.
Mouton, P.R., Gokhale, A.M., Ward, N.L., West, M.J., 2002. Stereological length estimation using spherical probes. J. Microsc. 206, 54–64.
Movshon, J.A., Lennie, P., 1979. Pattern-selective adaptation in visual cortical neurones. Nature 278, 850–852.
Mrzljak, L., Levey, A.I., Rakic, P., 1996. Selective expression of m2 muscarinic receptor in the parvocellular channel of the primate visual cortex. Proc. Natl. Acad. Sci. U. S. A. 93, 7337–7340.
Murphy, P.C., Sillito, A.M., 1991. Cholinergic enhancement of direction selectivity in the visual cortex of the cat. Neuroscience 40, 13–20.
Origlia, N., Kuczewski, N., Aztiria, E., Gautam, D., Wess, J., Domenici, L., 2006. Muscarinic acetylcholine receptor knockout mice show distinct synaptic plasticity impairments in the visual cortex. J. Physiol. 577, 829–840.
Palmer, S.M., Rosa, M.G., 2006. A distinct anatomical network of cortical areas for analysis of motion in far peripheral vision. Eur. J. Neurosci. 24, 2389–2405.
Paxinos, Franklin, 2012. Paxinos and Franklin's the Mouse Brain in Stereotaxic Coordinates, 4th edition. Academic Press.
Prusky, G.T., Shaw, C., Cynader, M.S., 1987. Nicotine receptors are located on lateral geniculate nucleus terminals in cat visual cortex. Brain Res. 412, 131–138.
Roberson, E.D., English, J.D., Adams, J.P., Selcher, J.C., Kondratick, C., Sweatt, J.D., 1999. The mitogen-activated protein kinase cascade couples PKA and PKC to cAMP response element binding protein phosphorylation in area CA1 of hippocampus. J. Neurosci. 19, 4337–4348.
Roberts, M.J., Zinke, W., Guo, K., Robertson, R., McDonald, J.S., Thiele, A., 2005. Acetylcholine dynamically controls spatial integration in marmoset primary visual cortex. J. Neurophysiol. 93, 2062–2072.
Rosa, M.G.P., Tweedale, R., 2004. Maps of the visual field in the cerebral cortex of primates: functional organization and significance. In: Kaas, J.H.C., C.E. (Eds.), The Primate Visual System. CRC Press, pp. 261–288.
Rouse, S.T., Marino, M.J., Potter, L.T., Conn, P.J., Levey, A.I., 1999. Muscarinic receptor subtypes involved in hippocampal circuits. Life Sci. 64, 501–509.
Salgado, H., Bellay, T., Nichols, J.A., Bose, M., Martinolich, L., Perrotti, L., Atzori, M., 2007. Muscarinic M2 and M1 receptors reduce GABA release by Ca^{2+} channel modulation through activation of PI3K/Ca^{2+}-independent and PLC/Ca^{2+}-dependent PKC. J. Neurophysiol. 98, 952–965.
Sato, H., Hata, Y., Masui, H., Tsumoto, T., 1987. A functional role of cholinergic innervation to neurons in the cat visual cortex. J. Neurophysiol. 58, 765–780.
Schuett, S., Bonhoeffer, T., Hubener, M., 2002. Mapping retinotopic structure in mouse visual cortex with optical imaging. J. Neurosci. 22, 6549–6559.
Series, P., Lorenceau, J., Fregnac, Y., 2003. The "silent" surround of V1 receptive fields: theory and experiments. J. Physiol. Paris 97, 453–474.
Sillito, A.M., 1975. The contribution of inhibitory mechanisms to the receptive field properties of neurones in the striate cortex of the cat. J. Physiol. 250, 305–329.
Sillito, A.M., 1977. The spatial extent of excitatory and inhibitory zones in the receptive field of superficial layer hypercomplex cells. J. Physiol. 273, 791–803.
Silver, M.A., Shenhav, A., D'Esposito, M., 2008. Cholinergic enhancement reduces spatial spread of visual responses in human early visual cortex. Neuron 60, 904–914.
Soma, S., Shimegi, S., Osaki, H., Sato, H., 2012. Cholinergic modulation of response gain in the primary visual cortex of the macaque. J. Neurophysiol. 107, 283–291.
Soma, S., Shimegi, S., Suematsu, N., Sato, H., 2013. Cholinergic modulation of response gain in the rat primary visual cortex. Sci. Rep. 3, 1138.
Thiele, A., 2013. Muscarinic signaling in the brain. Annu. Rev. Neurosci. 36, 271–294.
Ts'o, D.Y., Frostig, R.D., Lieke, E.E., Grinvald, A., 1990. Functional organization of primate visual cortex revealed by high resolution optical imaging. Science 249, 417–420.
Vanni, M.P., Provost, J., Lesage, F., Casanova, C., 2010. Evaluation of receptive field size from higher harmonics in visuotopic mapping using continuous stimulation optical imaging. J. Neurosci. Methods 189, 138–150.
Vanzetta, I., Grinvald, A., 1999. Increased cortical oxidative metabolism due to sensory stimulation: implications for functional brain imaging. Science 286, 1555–1558.
Vanzetta, I., Grinvald, A., 2008. Coupling between neuronal activity and microcirculation: implications for functional brain imaging. HFSP J. 2, 79–98.
Volpicelli, L.A., Levey, A.I., 2004. Muscarinic acetylcholine receptor subtypes in cerebral cortex and hippocampus. Prog. Brain Res. 145, 59–66.
Wess, J., 2004. Muscarinic acetylcholine receptor knockout mice: novel phenotypes and clinical implications. Annu. Rev. Pharmacol. Toxicol. 44, 423–450.
West, M.J., Slomianka, L., Gundersen, H.J., 1991. Unbiased stereological estimation of the total number of neurons in the subdivisions of the rat hippocampus using the optical fractionator. Anat. Rec. 231, 482–497.
Willshaw, D., 2006. Analysis of mouse EphA knockins and knockouts suggests that retinal axons programme target cells to form ordered retinotopic maps. Development 133, 2705–2717.
Wong, A.A., Brown, R.E., 2006. Visual detection, pattern discrimination and visual acuity in 14 strains of mice. Genes Brain Behav. 5, 389–403.
Yamada, M., Lamping, K.G., Duttaroy, A., Zhang, W., Cui, Y., Bymaster, F.P., McKinzie, D.L., Felder, C.C., Deng, C.X., Faraci, F.M., Wess, J., 2001. Cholinergic dilation of cerebral blood vessels is abolished in M(5) muscarinic acetylcholine receptor knockout mice. Proc. Natl. Acad. Sci. U. S. A. 98, 14096–14101.
Yazaki-Sugiyama, Y., Kang, S., Cateau, H., Fukai, T., Hensch, T.K., 2009. Bidirectional plasticity in fast-spiking GABA circuits by visual experience. Nature 462, 218–221.
Zhang, W., Basile, A.S., Gomeza, J., Volpicelli, L.A., Levey, A.I., Wess, J., 2002. Characterization of central inhibitory muscarinic autoreceptors by the use of muscarinic acetylcholine receptor knock-out mice. J. Neurosci. 22, 1709–1717.
Zhang, Z.W., Kang, J.I., Vaucher, E., 2011. Axonal varicosity density as an index of local neuronal interactions. PLoS One 6, e22543.
Zinke, W., Roberts, M.J., Guo, K., McDonald, J.S., Robertson, R., Thiele, A., 2006. Cholinergic modulation of response properties and orientation tuning of neurons in primary visual cortex of anaesthetized marmoset monkeys. Eur. J. NeuroSci. 24, 314–328.